



Research Repository UCD

Title	Mode I fracture toughness of co-cured and secondary bonded composite joints
Authors(s)	Mohan, Joseph, Ivankovic, Alojz, Murphy, Neal
Publication date	2014-06
Publication information	Mohan, Joseph, Alojz Ivankovic, and Neal Murphy. "Mode I Fracture Toughness of Co-Cured and Secondary Bonded Composite Joints." Elsevier, June 2014. https://doi.org/10.1016/j.ijadhadh.2014.02.008 .
Publisher	Elsevier
Item record/more information	http://hdl.handle.net/10197/5909
Publisher's statement	This is the author's version of a work that was accepted for publication in International Journal of Adhesion and Adhesives. Changes resulting from the publishing process, such as peer review, editing, corrections, structural formatting, and other quality control mechanisms may not be reflected in this document. Changes may have been made to this work since it was submitted for publication. A definitive version was subsequently published in International Journal of Adhesion and Adhesives (51, , (2014)) DOI: http://dx.doi.org/10.1016/j.ijadhadh.2014.02.008
Publisher's version (DOI)	10.1016/j.ijadhadh.2014.02.008

Downloaded 2025-12-04 23:02:25

The UCD community has made this article openly available. Please share how this access benefits you. Your story matters! (@ucd_oa)



© Some rights reserved. For more information

Mode I fracture toughness of co-cured and secondary bonded composite joints

J. Mohan^a, A. Ivanković^a, N. Murphy^{a,*}

^a*UCD Centre of Adhesion and Adhesives,
School of Mechanical & Materials Engineering, University College Dublin, Belfield, Dublin 4, Ireland.
Tel: +353 (0)1 716 1880, Fax: +353 (0)1 283 0534.*

Abstract

The mode I fracture toughness of a single co-cured and two secondary bonded joint systems were determined using the double cantilever beam test. The initiation values of fracture toughness from the PTFE film insert and a mode I crack-tip were considered as well as propagation values. It was found that the starting defect had a large influence on the initiation values for fracture toughness. It was also found that the two secondary bonded systems predominantly resulted in cohesive failure while the co-cured joint failed interfacially. Thermogravimetric analysis coupled with mass-spectrometry was used to show how moisture in the composite prepreg and adhesive affected the toughness of the joints. Microscopy methods were used to gain further insight into the damage mechanisms of the three joint systems.

Keywords: epoxy/epoxides, composites, adhesive joints, fracture mechanics, microscopy.

1. Introduction

In composite assemblies, adhesive joints are typically classified as secondary bonded, in which two precured laminates are bonded together, or co-cured, in which the laminate and adhesive are cured in a single processing operation. Prior to their use in critical load bearing components, a greater understanding of the fracture behaviour of these composite joint systems is required. Co-cured joints, for example, can suffer from problems associated

*Corresponding Author. Phone: +353 (0)1 716 1940, E-mail: neal.murphy@ucd.ie

with trapped water, both free and bound, being released during the co-curing process and adversely affecting the quality of the adhesive joint. The present study aims to investigate these problems by measuring the mode I fracture toughness of a single co-cured and two secondary bonded composite joint systems using the linear elastic fracture mechanics (LEFM) based double cantilever beam (DCB) test in accordance with the British Standard outlined in [1].

2. Materials & manufacture of joints

Two aerospace grade materials were used in the present study; a 180 °C cure unidirectional carbon-fibre/epoxy prepreg (CYCOM 977-2/HTS) and a 120 °C cure epoxy film adhesive (FM300-2M). Although the film adhesive cures at 120 °C, it has a wide processing window and is capable of being co-cured with 180 °C cure prepregs. The film adhesive contains a polyester scrim cloth with random fibre orientation that aids in handling and also in controlling the bondline thickness. Both materials were manufactured and supplied by Cytec Engineered Materials (CEM). The composite laminates and adhesive joints were produced in-house at UCD using a vacuum bagging layup procedure similar to that used in industry. Secondary bonded joints were produced by curing a single sheet of FM300-2M adhesive at either 120 °C or 180 °C between two pre-cured laminates. Each laminate consisted of 10 plies of 977-2/HTS. Prior to bonding, the laminates were grit-blasted to remove any release agent residue and also to roughen the surface which aids in adhesive bonding [2]. A 12 μm thick PTFE sheet was placed between the laminate and adhesive on one side of the layup to act as a crack initiator. Co-cured joints were produced in a similar fashion by curing the prepreg and the adhesive at the same time in a single process operation at 180 °C. For simplicity, the co-cured (CC) joint will be referred to as CC180, while the two secondary bonded (SB) joints will be referred to as SB180 and SB120, with the three digits referring to the cure temperature employed. Once cured, the bonded composite laminates were machined to size using a diamond grinding disc. The specimens were cut to a nominal width of 25 mm and length of 150 mm with an initial crack starter length of 45 mm from the load-line. The total thickness of each specimen was ≈ 5.6 mm with an adhesive layer

thickness of $\approx 0.25 \pm 0.05$ mm. The bond-gap thickness of the joint is controlled by the scrim cloth in the film adhesive. While the bond-gap can have a pronounced effect of the fracture toughness [3], it is not believed the variations seen in this study had a pronounced effect on the experimental results.

3. Experimental methods

3.1. Fracture test methods

Double cantilever beam (DCB) tests were conducted in accordance with the British Standard outlined in [1]. A Tinius-Olsen Hounsfield 50 kN (Model H50K-T UTM) screw-driven tensile test machine was used for the fracture tests. A 10 kN load cell was used to record the applied load. The crack length was monitored using a travelling microscope with $\times 10$ magnification. All tests were carried out at a constant crosshead displacement rate of 1 mm/min at room temperature. Three repeats were performed for each joint system. The fracture toughness, G_{IC} , was calculated using a corrected beam theory (CBT) analysis from Equation (1).

$$G_{IC} = \frac{3P\delta}{2B(a + \Delta_I)} \cdot \frac{F}{N} \quad (1)$$

where P is the load, δ the opening displacement, B the width of the specimen and a the crack length. F , N and Δ_I are correction factors for large displacements, load block effects and root rotation of the crack tip respectively and are based on several papers by Williams [4, 5, 6] and are detailed in [1]. Two starter defects were examined in the present study; the Teflon film insert and a mode I precrack. This resulted in 4 initiation values from each of the two starter defects as well as a propagation value for fracture toughness. The four initiation values are the visual onset of crack propagation (VIS), onset of non-linearity (NL) on the force-displacement trace, 5% increase in compliance ($C_0 + 5\%$) and maximum force (MAX). The initiation values are described in greater detail in [1].

3.2. Microscopy methods

Optical microscopy (OM) was performed using an Olympus GX51 Inverted Optical Microscope. After a fracture test, longitudinal sections were cut from the sample which were then set in a polymer mounting agent and then polished to a smooth surface finish. Scanning electron microscopy (SEM) was performed on the resulting fracture surfaces using a Hitachi TM-1000 Tabletop-Microscope. The TM-1000 uses a backscattered electron (BSE) detector and can provide images up to $\times 10,000$ magnification. Samples were gold coated prior to imaging to reduce charging.

3.3. Thermal characterisation methods

Differential thermal analysis (DTA) and thermogravimetric analysis (TGA) were performed on a Rheometric Scientific STA 1500. Small samples of each material (≈ 20 mg of adhesive and ≈ 30 mg of prepreg) were placed in a 6 mm diameter aluminium crucible. An empty crucible was used as a reference sample for DTA. The samples were held in a flowing nitrogen atmosphere throughout the analysis. Two different types of heating regimes, dynamic scans and simulated cure cycles, were used on the adhesive and prepreg materials. Dynamic scans, where the sample was heated from from 25°C to 350°C at a rate of $10^{\circ}\text{C}/\text{min}$, were used to determine glass transition temperature of the materials. Simulated cure cycles were used to determine the weight loss of the materials over the course of a cure cycle. During simulated cure cycles, the sample was heated from 25°C to 180°C at a rate of $1.5^{\circ}\text{C}/\text{min}$ and then held at 180°C for 2 hrs. This cure cycle was used for the prepreg and adhesive when cured at 180°C . However, since the adhesive has a processing window of between 120 and 180°C , a second simulated cure cycle was used to determine the weight loss characteristics when the adhesive was cured at 120°C . In this cure cycle, the sample was heated from 25°C to 120°C at a rate of $1^{\circ}\text{C}/\text{min}$ and then held at 120°C for 2 hrs.

A simulated cure cycle was also performed on prepreg and adhesive samples using a Thermal Analysis (TA) TGA Q500 with a Hiden Analytical HPR20 mass spectrometer (MS) gas flow analyser. The simulated cure cycle used on the prepreg is shown in Figure 1a (the red trace). During the heating regime, the intensity of the water vapour mass spectrum

was monitored over the course of the cure cycle, as shown from the blue trace in Figure 1a. As expected, an initial rise in the intensity of the water vapour was observed at the beginning the cure cycle, representing the release of free water, and again at 180 °C when the bound water is released [7, 8]. A sample of adhesive was also analysed using TGA-MS. The heating regime (red trace) and associated water release (blue trace) are shown in Figure 1b. It can be seen that the adhesive also stores both free and bound water although the intensity of water vapour detected is an order of magnitude lower than the previous case. However, it should be noted that the TGA-MS data presented here were not normalised by mass. These particular tests were used to confirm that water was indeed being released from the materials during cure. For a more meaningful indication of the percentage weight loss associated with the free and bound water, TGA data will be presented and discussed in Section 4.2.

3.4. *Uniaxial tensile tests*

The stress-strain behaviour of the bulk adhesive was determined from uniaxial tensile tests on dogbone shaped specimens. Six sheets of film adhesive were stacked and debulked (i.e. held under vacuum for approximately 30 min). Specimens were cut from the layup using a punch with dimensions that adhere to the ASTM-D-638-5-MET standard. The samples were then cured in an air circulated oven. A Tinius-Olsen Hounsfield 50K tensile test machine fitted with a 1 kN load cell was used to record the force. A clip-gauge with an 8.5 mm gauge length was used to record the strain. The specimen was loaded at a strain rate of $1 \times 10^{-3} \text{ s}^{-1}$.

4. Results & discussion

4.1. *Mode I initiation & propagation fracture toughness*

The type of defect in an adhesive joint or composite laminate can influence the initiation values of G_C [9, 10]. Two initial defects were examined in the present work; a 12 μm thick Teflon film insert and a mode I precrack. Figures 2a to 2c show the values of the four initiation criteria for each joint system when testing from the insert and precrack. Each

initiation value is based on an average of three specimens and the error bars represent plus and minus one standard deviation. The *NL* initiation point generally gives a more conservative value for initiation fracture toughness [11]. However, there are several factors that can influence the initiation values for fracture toughness and these will now be discussed.

The errors bars for the CC180 joint system are quite large compared to the two secondary bonded joints. This is possibly due to a ripple effect caused by the Teflon film insert during fabrication of the co-cured joint (see Figure 3). Note that the ripples are not present on either of the two secondary bonded joints. The larger error bars for the SB120 joint system compared to the SB180 joint are possibly due to the scrim cloth. It will be shown later that the SB120 joint system exhibits a much greater degree of scrim cloth fibre pull-out than the SB180 joint. Given the randomness of the scrim cloth weave, this would likely lead to a larger variation in initiation fracture toughness for the SB120 joint. It was found somewhat surprisingly that, with the single exception of the *MAX* initiation criterion for the SB180 joint system, the initiation values are all higher when testing from the precrack as opposed to the relatively blunt insert.

Figure 2d shows the mode I propagation fracture toughness for each joint system. The CC180 joint was the weakest while the SB120 joint was the toughest during crack propagation. After testing, the specimens were manually broken apart to examine the fracture surfaces. Figure 3 shows typical mode I fracture surfaces for each joint system. In the region where the fracture test was conducted, it can be seen that the co-cured joint failed interfacially while the two secondary bonded joints failed cohesively. It should be noted that there were some small areas where the co-cured joint failed cohesively which would positively contribute to the fracture toughness values.

4.2. Thermal characterisation analysis

After a fracture test, adhesive was scraped from the substrate and T_g was determined using DTA. Figure 4a shows the values of T_g for each joint system. Clearly, the curing conditions can greatly affect the glass transition temperature of the adhesive [12, 13]. Typically, it would be expected that the higher cure temperature of the SB180 joint system

would result in a higher T_g compared to the SB120 joint as others have reported [13]. In contrast, the adhesive taken from the SB180 joint system had a lower T_g than that from the SB120 joint. There was also a significant reduction in T_g of the adhesive when it was simultaneously cured with the prepreg in the CC180 joint.

Comparing the results to the propagation values of fracture toughness in Figure 2d, it appears that T_g is proportional to G_{IC} , which would seem to concur with the findings of Blackman et al [14]. However, in that work, the locus of failure remained cohesive, regardless of the level of pre-bond moisture, while in the present study, the locus of failure for the CC180 joint system was interfacial. As a result, T_g alone can not be used to fully explain the differences in initiation values for fracture toughness when testing from the Teflon film insert, particularly the SB120 joint system. This will be discussed shortly by considering the bulk tensile properties of the adhesive.

Kohli [12] used FM300-2K (the K denotes a woven scrim cloth) to bond aluminium substrates. That author reports little change in T_g with cure temperatures ranging from 120 °C to 180 °C. However, it should be noted that a consistent cure cycle was not used in that case, with a longer cure time being employed at the lower cure temperatures which gave similar values for T_g when cured at the higher temperatures for a shorter duration. As previously discussed, FM300-2M is a dual cure film adhesive for use in co-cured, co-bonded and secondary bonded applications with a wide variety of composite materials [15]. The adhesive was likely designed to have a flexible cure cycle to suit these demanding requirements. Zhao et al. [13] investigated the mode I adhesive fracture toughness of aluminium substrates bonded with FM300-2. The adhesive was cured at three temperatures; 120, 150 and 177 °C. The authors found that the joint cured at 120 °C was slightly tougher than that cured at 150 or 177 °C which is in agreement with the present work. However, the authors used metallic substrates and consequently there were no moisture dominated effects. This resulted in the adhesive being more brittle when cured at 177 °C as opposed to 120 °C (i.e. higher T_g when cured at the elevated temperature). The authors proposed that the increased ductility of the adhesive when cured at 120 °C led to increased energy absorption and, hence, a higher G_C . However, it should also be noted that the use of metallic substrates in that work, as

opposed to the CFRP substrates employed in the present study, would likely lead to very different temperature histories between the different substrates, even if they are cured using the same cure cycle.

The lower T_g of the CC180 system suggests an extra effect other than that of cure temperature on the adhesive. Epoxy resin systems are known to retain small amounts of bound water [7, 8, 16] that could potentially be released during the cure cycle, plasticising the adhesive and potentially interfering with the cross-linking process, thereby reducing T_g . A simulated cure cycle (see Figure 5a) of the prepreg shows two distinct regions of weight loss, the first due to release of free water and the second due to bound water. This would imply that the bound water is released during co-curing of the prepreg, a phenomenon which does not occur during the secondary bonding operation. The release of the additional water vapour explains the lower T_g of the CC180 joint system. It should be noted that the differences in T_g reported here are likely the result of a combination of both the cure temperature and prebond moisture stored in the prepreg, laminate or adhesive before curing [14]. While the experimental data from the thermal characterisation methods suggest that the adhesive has been plasticised due to diffusion of the water from the prepreg into the adhesive, it would be advantageous to model the diffusion process to determine if it is possible during the time span of a cure cycle (4 hrs). While such a study is beyond the scope of the present work, it is expected that the elevated heat and pressure would accelerate any diffusion process.

The weight loss trace of the adhesive over the course of a 180 °C and 120 °C simulated cure cycle are shown in Figures 5b and 5c respectively. Thermogravimetric analysis with mass spectrometry showed that the adhesive also contained both free and bound water (see Figure 1b). During curing of the CC180 joint, both free and bound water are expected to be released from both the prepreg and adhesive. However, during preparation of the two secondary bonded systems, the moisture in the prepreg, both free and bound, has already been released. The only moisture remaining is that in the adhesive. The weight loss traces and mass spectrometer results obtained from TGA/TGA-MS suggest that only free water would affect the glass transition temperature of the adhesive in the SB120 joint system

while the SB180 system would be affected by both the free and bound water stored in the adhesive. It will be shown in the next Section that the glass transition temperature of the FM300-2M film adhesive is approximately 150 °C when cured at 120 °C in an air-circulated oven for 2 hrs. This is very close to that of the adhesive taken from the SB120 joint system. This suggests that the SB120 joint system does not suffer from a significant reduction in T_g due to the release of free water during the cure cycle. It also suggests that the depression in T_g of the SB180 joint system can be attributed to the bound water. The fact that the adhesive was confined between the composite laminates in the layup may have prevented the free and, particularly, the bound water in the adhesive escaping during the curing process which could have led to the depression of T_g in the SB180 joint system. This could have been caused by inadequate ventilation of the vacuum bag during the cure cycle, as can occur in industry [17]. Whether or not the free and bound water remain in the SB180 & SB120 joint systems after cure is unclear. It may be the case that the released water interferes with the polymerisation of the adhesive during cure [8] or plasticises the adhesive. If it is the latter, then drying the joint system, in a heated vacuum desiccator for example, should be able to reverse the plasticisation [26]. However, this was not examined in the present study. It should also be noted that there may have been residual moisture left in the composite laminate or that the laminate reabsorbed moisture from the atmosphere in the few hours during preparation of the secondary bonded joints that could also have affected the glass transition temperature and fracture toughness [14].

4.3. Tensile properties of bulk adhesive specimens

The tensile properties of the adhesive can be used to gain an insight into the differences in the initiation values for fracture toughness when testing from the Teflon film insert or mode I precrack. An attempt was made to match the glass transition temperature of the bulk adhesive dogbone specimens with those of the different joint systems. T_g of this particular adhesive depends greatly on both the cure temperature and the cure time. FM300-2M is often cured for longer times at lower cure temperatures to achieve a comparable value for T_g when cured at high temperatures for a shorter time [12]. By curing the adhesive for

2 hrs at 120 °C in an air-circulated oven, a T_g of approximately 150 °C was obtained which would be comparable to the SB120 joint system. When the adhesive was cured at 180 °C for 1 hr, a T_g of 143 °C was obtained which agreed well with the SB180 joint system. To prepare dogbone specimens comparable to the CC180 joint system, it was necessary to age the samples in hot deionised water. In this case, the adhesive was also cured at 180 °C for 1 hr prior to ageing. Figure 4b shows the effect of the duration of ageing on the glass transition temperature of the dogbone specimens. An ageing time of 2 hrs yielded a similar T_g to that of the CC180 joint system. The method of modifying the glass transition temperature of the bulk adhesive specimens was chosen under the assumption that the plasticisation was due to water being released during the cure cycle and would therefore reflect the curing conditions encountered during manufacture of the composite joints (i.e. different cure temperatures for the specimens representing the SB180 and SB120 joint systems and plasticisation due to water for the CC180 specimens). However, it should be noted that there are many factors that can influence T_g in polymers. It has already been shown in this work that the glass transition temperature of FM300-2M is greatly affected by both the curing temperature and time. The molecular weight, chemical structure, level of copolymerisation and degree of crosslinking can all have an effect on the glass transition temperature [18]. When water is introduced into an adhesive, bound water can raise T_g while free water can lower it [7, 8]. Moisture can also displace the polymer chains and swell the polymer leading to chemical compaction of the material, as noted by Zhou and Lucas [8]. As a result, the bulk adhesive material produced using this method may not be an exact match of that produced in the cured composite joints.

Figure 6 shows the stress-strain curves for the dogbone specimens that represent each of the three joint systems. As expected, the mechanical properties are clearly dependent on the glass transition temperature. The stiffness is proportional to T_g , as has been reported elsewhere [19], with the specimens representing the SB120 joint system (T_g of 150 °C) being less compliant than those of the CC180 system (T_g of 137 °C). The specimens representing the SB120 joint system also have the highest failure stress while the CC180 specimens have the highest strain at failure. The SB180 tensile specimens have comparable failure stresses

to the CC180 specimens but exhibit a slightly lower failure strain.

4.4. Microscopy analysis

To understand the differences between the initiation values when testing from the Teflon film insert or precrack, it is beneficial to examine the cross-sections of the two defect types. A micrograph was taken of the region at the tip of the Teflon film insert in an SB120 joint system and can be seen in Figure 7. A second specimen was precracked 5 mm ahead of the Teflon film insert. The test was then stopped and a section from the centre of the specimen (i.e. the cross-section would represent plane strain conditions) was cut out and prepared for optical microscopy. Figure 8 shows a series of micrographs taken of the crack path from the Teflon film insert. In Figures 7 and 8, the white lines at the top and bottom of each micrograph are the carbon-fibres of the composite substrate and the distinctive trilobal cross sections are the individual fibres of the scrim cloth in the film adhesive.

The defect in Figure 7 is a relatively blunt notch compared to that of the precrack in Figure 8. It is likely that initiation values for fracture toughness from the Teflon film insert are dominated by bulk plasticity ahead of the blunt crack tip. If this is the case, then the initiation values presented in Figures 2a to 2c would be governed by the tensile stress-strain properties of the adhesive. Referring back to Figure 6, the dogbone specimens representative of the SB120 joint system are noticeably stiffer, particularly at higher stresses. Two stress-strain curves are taken from Figure 6 that represent the SB180 and SB120 joint systems. These curves are shown in Figure 9a and 9b respectively. The competition between fracture and plasticity is governed by the relation between σ_{yield} and σ_{max} [20, 21]. Note that the maximum stress is simply the highest stress before failure (i.e. the stress at the final point on the stress-strain curve) while the yield point is defined by the 0.2% proof. If these two values are very close, then there will be little plasticity before fracture. However, if the yield stress is much lower than the maximum stress, then there will be plastic flow which will lead to increased energy absorption and higher toughness, as is the case for the SB180 and CC180 joint systems. This corresponds well with the initiation values for fracture toughness and offers a possible explanation for the lower initiation values of the SB120 joint system.

However, the stress-strain curves do not correlate with the initiation values from the mode I precrack or the propagation fracture toughness. These values appear to be proportional to the glass transition temperature of the adhesive (see Figures 2d and 4a). Blackman et al. [14] reported a similar result for propagation values of fracture toughness.

The initiation values when testing from the precrack are governed by a more complex fracture process that involves the scrim cloth, which is known to influence damage mechanisms in adhesive joints [22, 23, 24], and also the locus of failure, which can also have an effect [22]. When the crack begins to propagate from the Teflon film insert, it is possible that the specimen may exhibit R-curve behaviour due to an evolving damage zone. Figure 10 shows a plot of G_{IC} versus crack length for the first 5 mm of crack growth recorded during the precracking stage of the mode I DCB test. It can be seen that the two secondary bonded joints show evidence of R-curve behaviour while the co-cured does not. The mode I precrack defect, as shown in Figure 8 for the SB120 joint system, is more akin to multiple sharp cracks, that all appear to initiate at a scrim cloth fibre.

The R-curve in Figure 10 suggests that this damage zone evolves over several millimetres of crack growth from the blunt Teflon film and leads to higher initiation values for fracture toughness when testing from the mode I precrack. It is possible that it takes considerably more energy to initiate crack growth from this fully developed damage zone than from one blunt crack, as is the case when testing from the Teflon insert (previously shown in Figure 7). These individual cracks eventually coalesce into one main crack, as can be seen in Figure 8a. The first stage in crack growth appears to be debonding of the adhesive from the scrim cloth fibres. This creates regions that amplify the applied stress and encourages crack growth. It is interesting to note that these debonded regions seem to communicate with each other, with cracks appearing to grow against the main direction of propagation. These processes are highlighted in Figure 8f. The lack of R-curve behaviour for the CC180 joint system is likely due to the fact that the co-cured joint failed interfacially. During interfacial crack propagation, the scrim cloth will play a diminished role in the energy absorption mechanisms and so will not contribute to an evolving damage zone.

This highlights the fact that initiation values, as well as the resulting R-curve behaviour,

from crack-starter films can be misleading and not representative of a damage evolution from a real-life crack-tip. As a result, it is usually more appropriate to quote the propagation value, when self-similar crack growth has been achieved, as a more representative value of the true fracture toughness. The accuracy of this analysis can be further improved by using a crack equivalent procedure, such as that employed by Morais et al. [25]. This eliminates the need to visually monitor the crack length, which can be difficult during the initial region of R-curve behaviour.

Another series of optical micrographs was taken of each of the three joint systems as shown in Figure 11. These were prepared from longitudinal sections cut from tested DCB specimens (i.e. the substrates were fully separated), unlike the micrographs in Figure 8. Figure 11a shows the mode I crack path taken by the CC180 joint system. Regions of interfacial failure (with an associated low value of G_C), and smaller regions of cohesive failure are visible. The two secondary bonded joint systems result in cohesive failure with adhesive remaining on both substrates as shown in Figures 11b and 11c. The SB120 joint system also exhibits more scrim fibre pull-out than the CC180 or SB180 joint systems. The scrim fibres that have been pulled out can be seen suspended in the polymer mounting agent. A photograph of each joint system was taken at the end of the DCB test when the crack length was 115 mm. These photographs are shown in Figure 12. This Figure clearly shows extensive scrim cloth fibre-bridging in the SB120 joint during crack propagation which extends approximately 2.5 cm behind the crack tip which would positively contribute to the measured fracture toughness, G_C .

The cause behind this fibre-bridging was investigated in more detail using SEM. Samples of the scrim cloth were prepared by dissolving away the epoxy resins using dichloromethane. These samples were then subjected to two different heating regimes representative of the cure cycles used in preparation of the secondary bonded joints. The first was heated from room temperature to 180 °C at a rate of 3 °C/min and then held at this temperature for 1 hr. The second heating regime was identical to the first except it was held at 120 °C for 1 hr. The samples were subsequently gold coated and examined under the table top SEM. Figure 13a shows a series of micrographs of the sample heated to 180 °C. It can be seen

that there are a number of regions where the polyester fibres have fused together. This behaviour is not seen to the same extent in the samples heated to 120 °C (Figure 13b). It is proposed that the higher cure temperature used in the manufacture of the SB180 joint may have lead to a fusion of the scrim cloth and epoxy adhesive. This is similar to a problem encountered in the removal of some nylon peel plies from high temperature cure epoxy preregs [17]. The peel ply becomes bonded so strongly to the cured epoxy that removal from the laminate becomes difficult if not impossible. However, during crack propagation, this same fusion would likely prevent excessive scrim cloth fibre pull-out and fibre-bridging during crack propagation. These two damage mechanisms usually increase the size of the damage zone around the crack-tip and increase the fracture toughness of the joint.

The last point to be addressed is the difference in the locus of failure between the co-cured and the two secondary bonded joints. It has been shown that the low glass transition temperature of the CC180 joint system was due to moisture being released during the co-curing cycle. However, this release of moisture has a secondary effect of creating multiple voids at the adhesive-substrate interface. Figure 14a shows a cross section of the bondline of a CC180 joint. At higher magnifications, the voids at the interface are clearly visible. These voids are not seen to the same extent in the two secondary bonded joints (see Figures 14b and 14c).

Two regions of interest were examined: a representative band in the centre of the adhesive layer and the adhesive-substrate interface. The number of voids in these regions were manually counted for each joint system and are presented in Table 1. It can be seen that the CC180 joint system does indeed have a considerably larger number of voids in both the bulk adhesive and at the interface. It is extremely likely that these voids would weaken the interfacial fracture toughness below that of the cohesive strength of the adhesive and encourage crack growth at the adhesive-substrate interface. The two secondary bonded systems have comparable quantities of voids in both regions.

5. Conclusions

The mode I initiation values were found to be highly dependent on both the type of starter defect (insert versus precrack) and on the type of joint (co-cured versus secondary bonded). While the initiation values from the Teflon film insert were found to be governed by the tensile stress-strain properties of the adhesive, the propagation values were more associated with the damage mechanisms surrounding the scrim cloth fibres and locus of failure. The cause of these differences was found to be the fabrication methods used. The co-curing process released any free and bound water into the adhesive layer which was found to plasticise the polymer and introduce voids at the interface. During secondary bonding, the free and bound water would already have been released from the prepreg during fabrication of the laminates. As a result, the SB180 joint system would only be adversely affected by the free and bound water in the adhesive while the SB120 system would only be influenced by the free water. The differences in observed scrim fibre pull-out between the two secondary bonded joint systems were believed to be due to the elevated cure temperature causing melting and fusing of the scrim fibres to both themselves and the epoxy adhesive, thus preventing pull-out in the SB180 system.

It should be noted that there are several other factors that may have influenced the performance of the different joint systems such as the temperature histories during cure or the interaction between the chemical components of the composite and adhesive resins. However, the present work has shown that the contribution of free and bound water are an important factor and should be taken into account during fabrication of co-cured and secondary bonded composite joints.

Acknowledgements

The authors would like to gratefully acknowledge the financial support of the Irish Research Council for Science, Engineering and Technology (IRCSET) and Cytac Engineered Materials (CEM). The materials provided by CEM are also gratefully acknowledged.

References

- [1] BS-7991-2001. Determination of the mode I adhesive fracture energy, G_{IC} , of structural adhesives using the double cantilever beam (DCB) and tapered double cantilever beam (TDCB) specimens, 2001.
- [2] J. W. Chin and J. P. Wightman. Surface characterization and adhesive bonding of toughened bis-maleimide composites. *Composites: Part A*, 27A:419–428, 1996.
- [3] V. Cooper, A. Ivankovic, A. Karac, D. McAuliffe and N. Murphy. Effects of bond gap thickness on the fracture of nano-toughened epoxy adhesive joints. *Polymer*, 53(24):5540–5553, 2012.
- [4] J. G. Williams. On the calculation of energy release rates for cracked laminates. *International Journal of Fracture*, 36:101–119, 1988.
- [5] J. G. Williams. The fracture mechanics of delamination tests. *Journal of strain analysis*, 24(4):207–214, 1989.
- [6] S. Hashemi, A. J. Kinloch, and J. G. Williams. The analysis of interlaminar fracture in uniaxial fibre-polymer composites. *Proceedings of the Royal Society of London*, 427:173–199, 1990.
- [7] J. Zhou and J. P. Lucas. Hygrothermal effects of epoxy resin. Part I: the nature of water in epoxy. *Polymer*, 40:5505–5512, 1999.
- [8] J. Zhou and J. P. Lucas. Hygrothermal effects of epoxy resin. Part II: variations of glass transition temperature. *Polymer*, 40:5513–5522, 1999.
- [9] D. Stevanovic, S. Kalyanasundaram, A. Lowe, and P. Y. B. Jar. Effect of starting defect for interlaminar fracture testing of interlayer-toughened fiber reinforced composites. *Journal of Material Science Letters*, 20:629, 2001.
- [10] A. B. Pereira, A. B. de Morais, M. F. S. F. de Moura, and A. G. Magalhaes. Mode I interlaminar fracture of woven glass/epoxy multidirectional laminates. *Composites: Part A*, 36:1119–1127, 2005.
- [11] B. R. K. Blackman, A. J. Kinloch, M. Paraschi, and W. S. Teo. Measuring the mode I adhesive fracture energy, G_{IC} , of structural adhesive joints: the results of an international round-robin. *International Journal of Adhesion and Adhesives*, 23:293–305, 2003.
- [12] D. K. Kohli. Improved 121°C curing epoxy film adhesive for composite bonding and repair applications: FM300-2 adhesive system. *International Journal of Adhesion and Adhesives*, 19:231–242, 1999.
- [13] W. Zhao, K. Ramani, and B. E. Mueller. Processing and fracture behavior of a polyethylene-based thermoplastic adhesive and a glass-fiber filled epoxy adhesive. *International Journal of Adhesion and Adhesives*, 20:409–413, 2000.
- [14] B. R. K. Blackman, B. B. Johnsen, A. J. Kinloch, and W. S. Teo. The effects of pre-bond moisture on the fracture behaviour of adhesively-bonded composite joints. *Journal of Adhesion*, 84:256–276, 2008.
- [15] FM300-2M Material Specification. <http://www.cytec.com>. [Last Accessed 26th March 2012].
- [16] Y. C. Lin and X. Chen. Investigation of moisture diffusion in epoxy system: Experiments and molecular

- dynamics simulations. *Chemical Physics Letters*, 412:322–326, 2005.
- [17] L. J. Hart-Smith. An engineer asks: Is it really more important that paint stays stuck on the outside of an aircraft than that glue stays stuck on the inside? *The Journal of Adhesion*, 82:181–214, 2006.
 - [18] P. C. Painter and M. M. Coleman. *Fundamentals of Polymer Science: An Introductory Text*. Technomic Publishing, 1997.
 - [19] G. LaPlante and P. Lee-Sullivan. Moisture effects on FM300 structural film adhesive: Stress relaxation, fracture toughness, and dynamic mechanical analysis. *Journal of Applied Polymer Science*, 95:1285–1294, 2005.
 - [20] V. Tvergaard and J. W. Hutchinson. The relation between crack growth resistance and fracture process parameters in elastic-plastic solids. *Journal of the Mechanics and Physics of Solids*, 40:1377–1392, 1992.
 - [21] N. Murphy and A. Ivanković. The prediction of dynamic fracture evolution in PMMA using a cohesive zone model. *Engineering Fracture Mechanics*, 72(6):861–875, 2005.
 - [22] H. Parvatareddy and D. A. Dillard. Effect of mode-mixity on the fracture toughness of Ti-6Al-4V/FM-4 adhesive joints. *International Journal of Fracture*, 96:215–228, 1999.
 - [23] M. S. Forte, J. M. Whitney, and G. A. Schoeppner. The influence of adhesive reinforcement in Mode I fracture toughness of a bonded joint. *Composites Science and Technology*, 60:2389–2405, 2000.
 - [24] M. U. Jastrzebski, A. N. Sinclair, D. D. Raizenne, and J. K. Spelt. Development of adhesive bonds with reduced fracture strength as NDE benchmarks. *International Journal of Adhesion and Adhesives*, 29(4):372–379, 2009.
 - [25] J.J.L. Morais, M.F.S.F. de Moura, F.A.M. Pereira, J. Xavier, N. Dourado, M.I.R. Dias and J.M.T. Azevedo. The double cantilever beam test applied to mode I fracture characterization of cortical bone tissue. *Journal of the Mechanical Behavior of Biomedical Materials*, 3(6):446–453, 2010.
 - [26] A. Mubashar, I. A. Ashcroft, G. W. Critchlow, and A. D. Crocombe. Moisture absorption-desorption effects in adhesive joints. *International Journal of Adhesion and Adhesives*, 29(8):751–760, 2009.

List of Tables

Table 1: Number of voids in a representative band in the bulk adhesive and at the adhesive-substrate interface for each joint system.

Table 1: Number of voids in a representative band in the bulk adhesive and at the adhesive-substrate interface for each joint system.

Joint System	Bulk	Interface
CC180	103	48
SB180	57	13
SB120	50	12

List of Figures

Figure 1: TGA-MS of water released from (a) prepreg and (b) adhesive during the course of a cure cycle.

Figure 2: (a)-(c): Initiation values (based on three repeats) for each joint system when testing from the insert film and the mode I precrack. (d): Propagation values for the three composite joint systems (based on approximately 75 propagation points from the R-curves of three DCB tests).

Figure 3: Typical fracture surfaces of the three joint systems. The direction of crack propagation was from left to right. Regions corresponding to crack growth propagation are boxed in blue, where the specimen was manually broken apart in black and where adhesive was scraped away for DTA in red.

Figure 4: (a): T_g of adhesive scrapings taken from each joint system. Bars represent average of three measurements and error bars represent the absolute range. (b): T_g of adhesive cured at 180 °C for 1 hr and aged in deionised water at 75 °C.

Figure 5: Typical weight loss traces from simulated cure cycles for prepreg and adhesive.

Figure 6: Stress-strain curves of bulk adhesive specimens representative of the three joint systems (based on equivalent T_g).

Figure 7: Teflon insert in a SB120 joint prior to pre-cracking.

Figure 8: Series of optical micrographs showing the crack path during the *testing from insert* phase of a DCB test for a SB120 joint. Micrographs show approximately 5 mm of crack propagation. Each micrograph slightly overlaps the previous. Numbered red lines indicate distance from insert film. Note that (e) and (f) are the same micrograph with additional labels added for clarity. Here the crack propagates from left to right.

Figure 9: Stress-strain curves representative of the SB180 and SB120 joint systems. The 0.2% proof yield point and ultimate tensile strength are shown.

Figure 10: R-curve behaviour during mode I testing from the Teflon film insert for each joint system. Triangles represent the *VIS* initiation point and circles are propagation points.

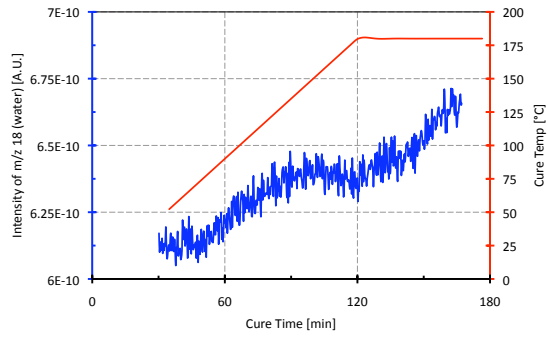
Figure 11: Mode I crack path of each joint system. Direction of crack propagation was from

left-to-right in each micrograph

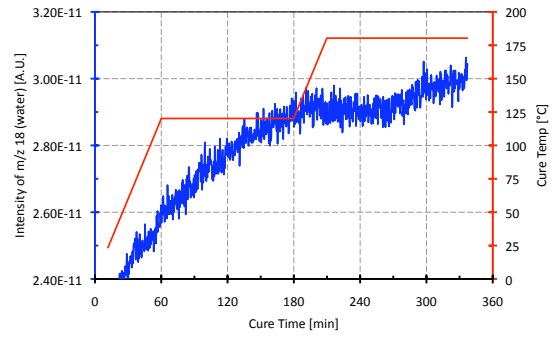
Figure 12: Photographs showing scrim cloth fibre-bridging in each of the three joint systems during a mode I DCB test. The CC180 & SB180 joints show relatively little bridging compared to the SB120 system. The photographs were taken at the end of the DCB test. The boxes at the bottom of the Figure indicate the crack length, a , at specified points.

Figure 13: SEM of scrim cloth fibres after being heated in STA1500 at (a): 180 °C and (b): 120 °C.

Figure 14: SEM image of adhesive-substrate interface of each joint system. Magnification is $\times 10000$.



(a) Prepreg.



(b) Adhesive.

Figure 1: TGA-MS of water released from (a) prepreg and (b) adhesive during the course of a cure cycle.

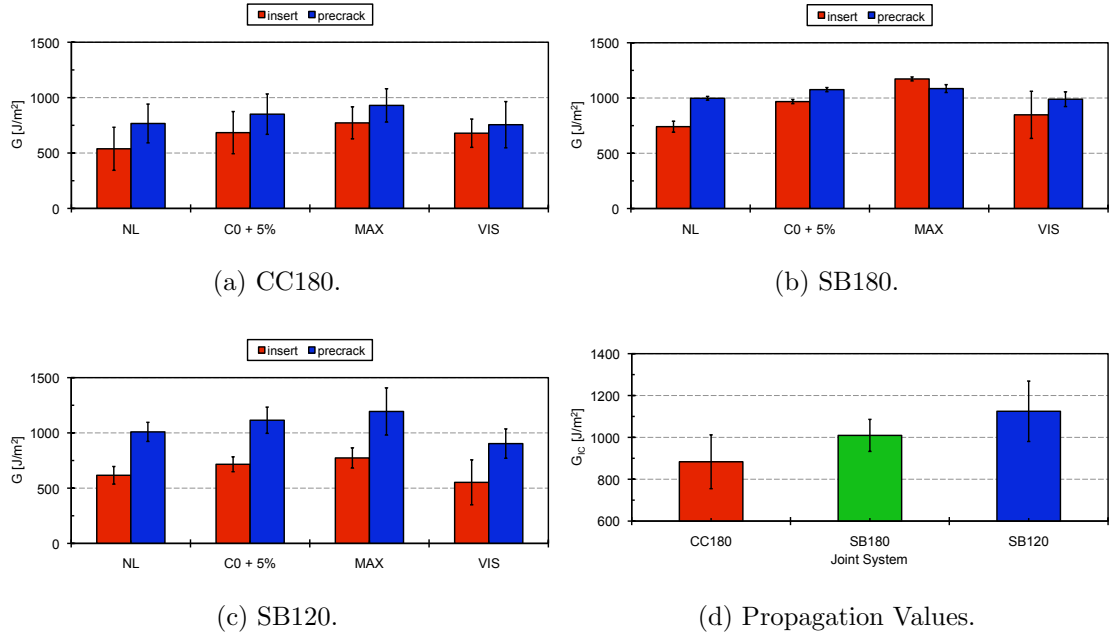


Figure 2: (a)-(c): Initiation values (based on three repeats) for each joint system when testing from the insert film and the mode I precrack. (d): Propagation values for the three composite joint systems (based on approximately 75 propagation points from the R-curves of three DCB tests).

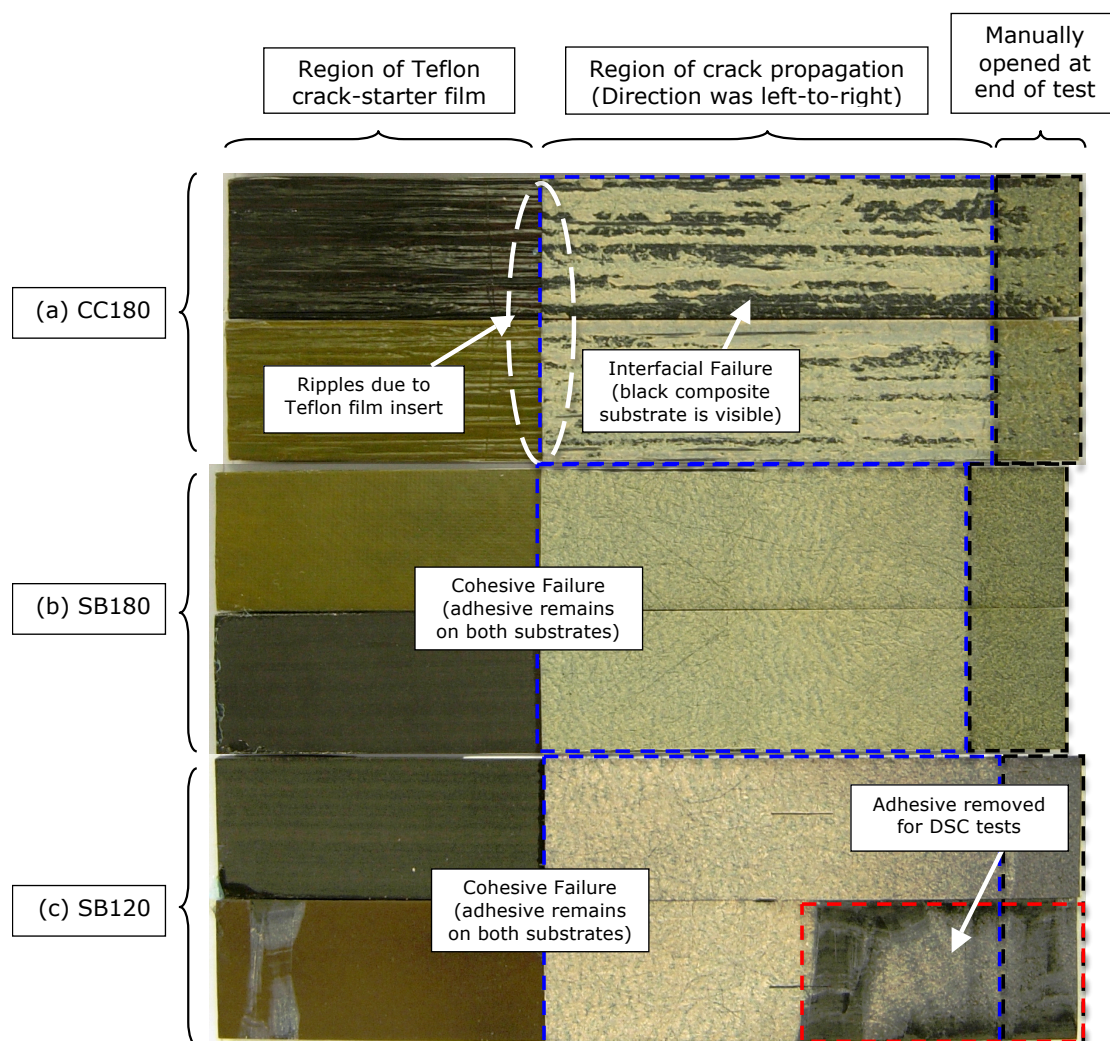
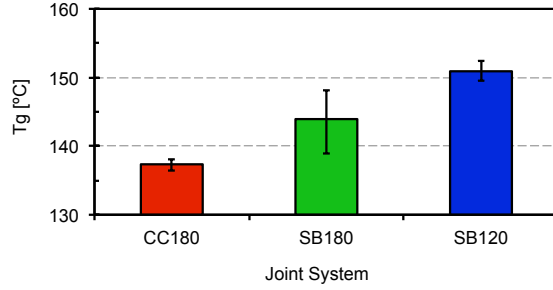
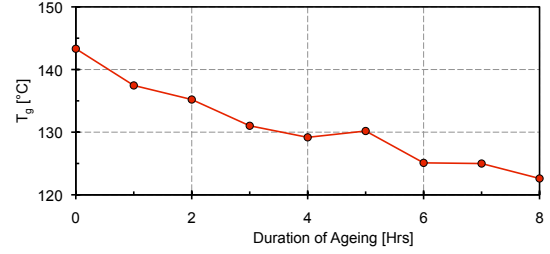


Figure 3: Typical fracture surfaces of the three joint systems. The direction of crack propagation was from left to right. Regions corresponding to crack growth propagation are boxed in blue, where the specimen was manually broken apart in black and where adhesive was scraped away for DTA in red.

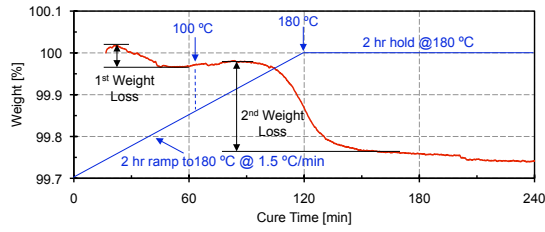


(a) Three joint systems.

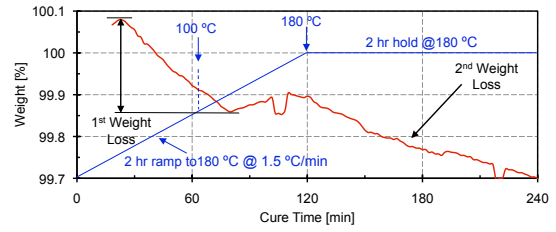


(b) Aged adhesive.

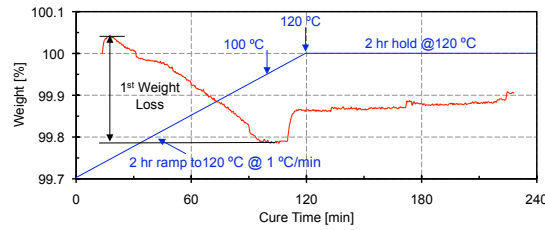
Figure 4: (a): T_g of adhesive scrapings taken from each joint system. Bars represent average of three measurements and error bars represent the absolute range. (b): T_g of adhesive cured at 180 °C for 1 hr and aged in deionised water at 75 °C.



(a) Prepreg.



(b) Adhesive cured at 180 °C.



(c) Adhesive cured at 120 °C.

Figure 5: Typical weight loss traces from simulated cure cycles for prepreg and adhesive.

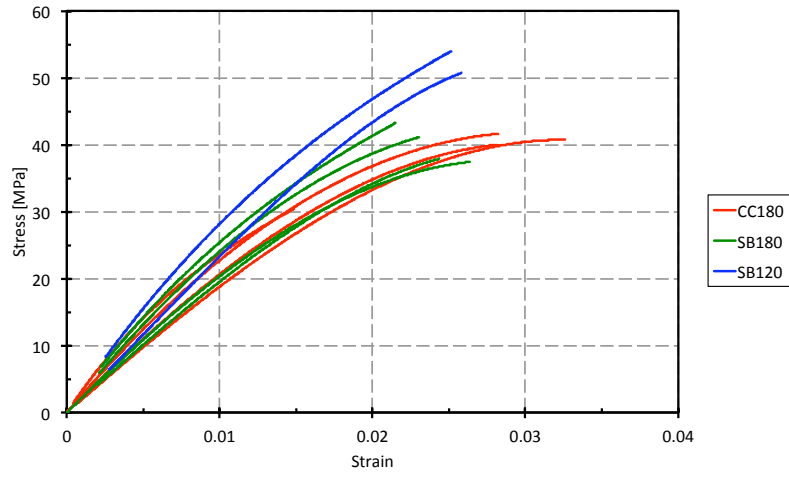


Figure 6: Stress-strain curves of bulk adhesive specimens representative of the three joint systems (based on equivalent T_g).

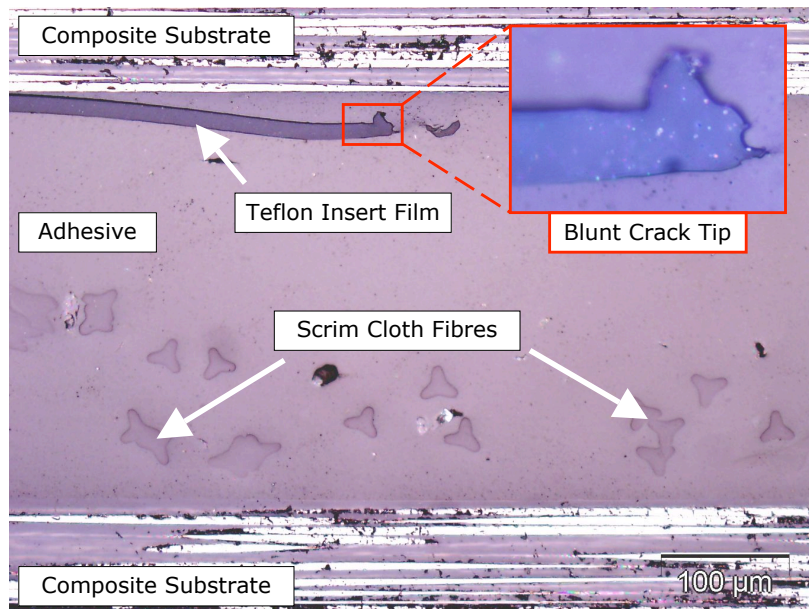


Figure 7: Teflon insert in a SB120 joint prior to pre-cracking.

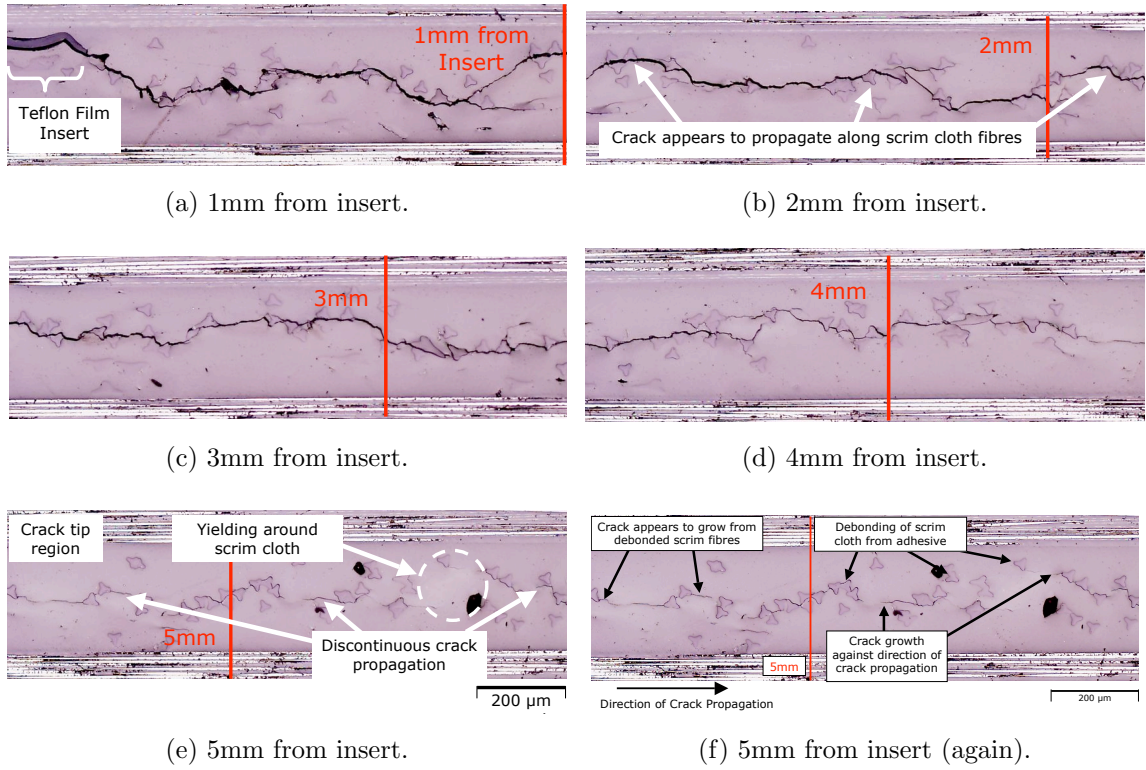


Figure 8: Series of optical micrographs showing the crack path during the *testing from insert* phase of a DCB test for a SB120 joint. Micrographs show approximately 5 mm of crack propagation. Each micrograph slightly overlaps the previous. Numbered red lines indicate distance from insert film. Note that (e) and (f) are the same micrograph with additional labels added for clarity. Here the crack propagates from left to right.

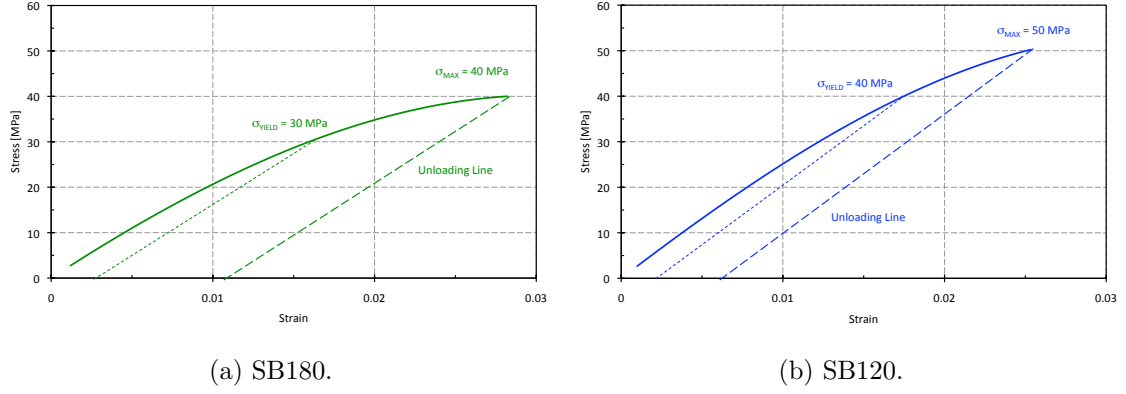


Figure 9: Stress-strain curves representative of the SB180 and SB120 joint systems. The 0.2% proof yield point and ultimate tensile strength are shown.

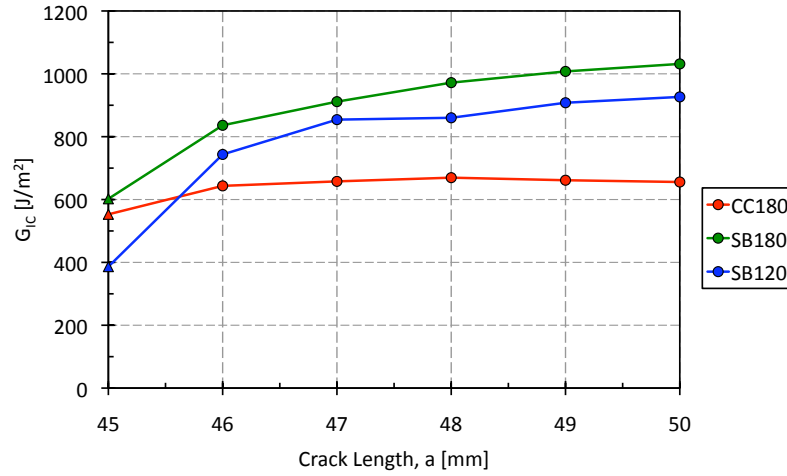
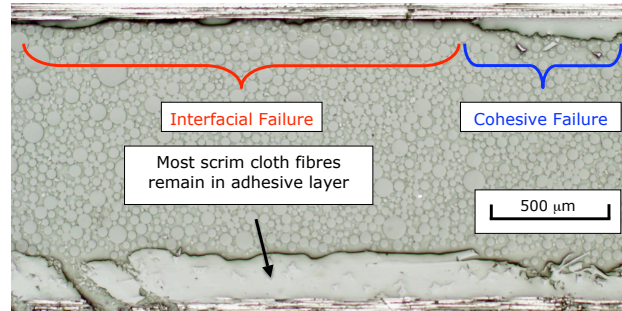
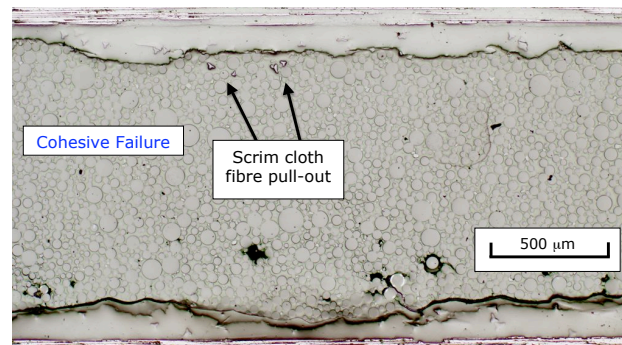


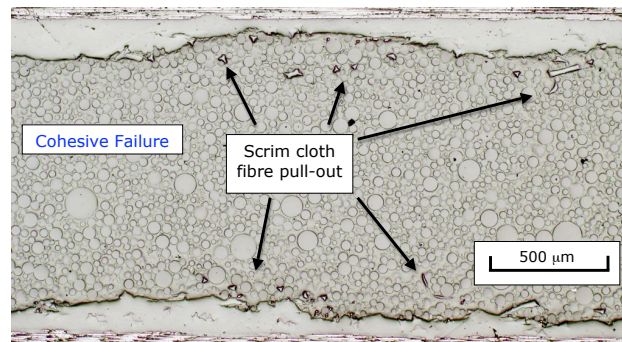
Figure 10: R-curve behaviour during mode I testing from the Teflon film insert for each joint system. Triangles represent the *VIS* initiation point and circles are propagation points.



(a) CC180.



(b) SB180.



(c) SB120.

Figure 11: Mode I crack path of each joint system. Direction of crack propagation was from left-to-right in each micrograph

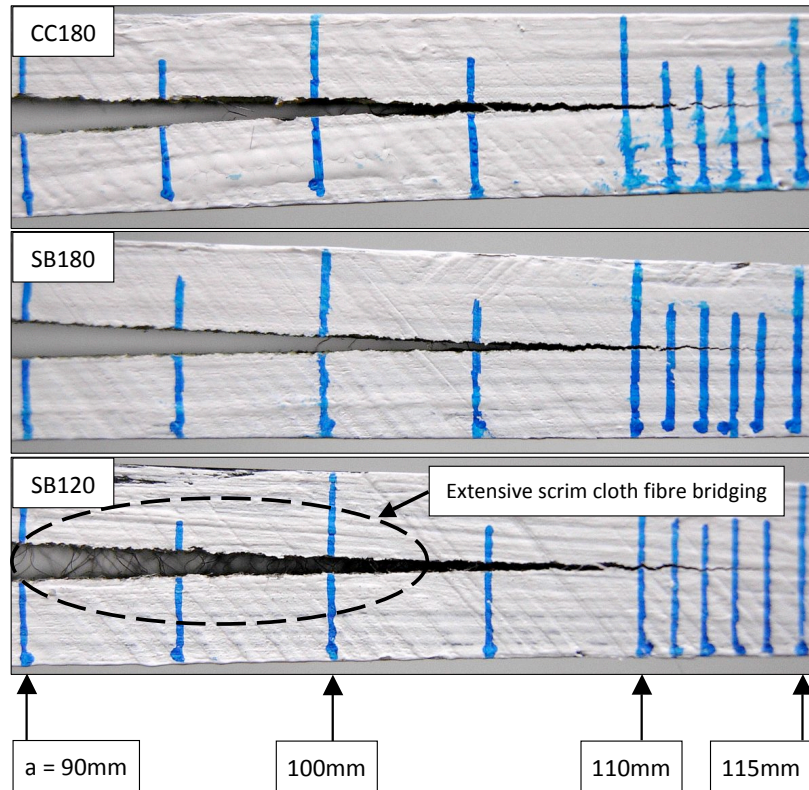


Figure 12: Photographs showing scrim cloth fibre-bridging in each of the three joint systems during a mode I DCB test. The CC180 & SB180 joints show relatively little bridging compared to the SB120 system. The photographs were taken at the end of the DCB test. The boxes at the bottom of the Figure indicate the crack length, a , at specified points.

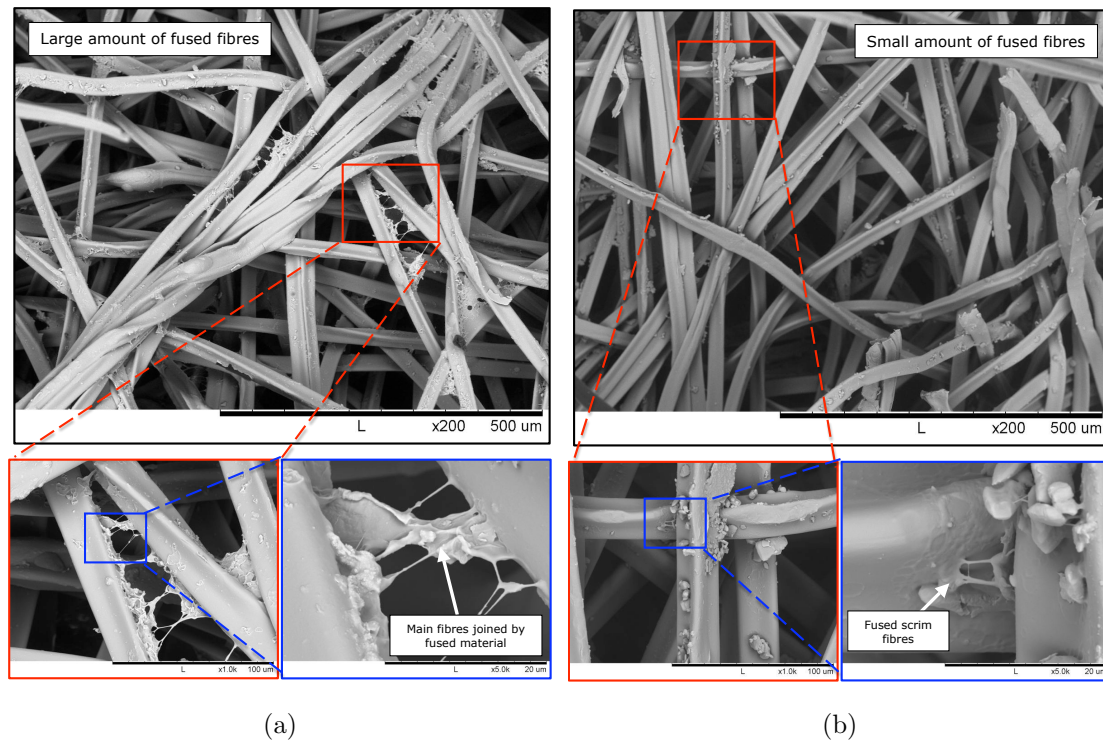
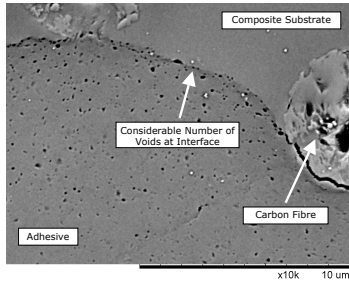
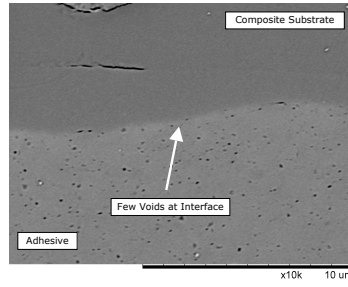


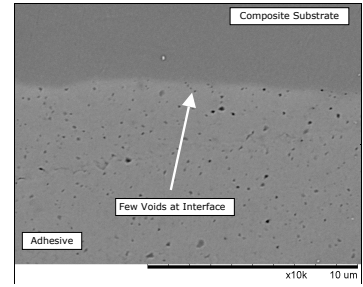
Figure 13: SEM of scrim cloth fibres after being heated in STA1500 at (a): 180 °C and (b): 120 °C.



(a) CC180.



(b) SB180.



(c) SB120.

Figure 14: SEM image of adhesive-substrate interface of each joint system. Magnification is $\times 10000$.